2019

Two-photon microperimetry: Sensitivity of human photoreceptors to infrared light

Daniel Ruminski
Case Western Reserve University

Grazyna Palczewska
Polgenix, Inc.

Maciej Nowakowski
AM2M LLC LP

Agnieszka Zielińska
Nicolaus Copernicus University of Torun

Vladimir J Kefalov
Washington University School of Medicine in St. Louis

See next page for additional authors

Research Article | Vol. 10, No. 9 / 1 September 2019 / Biomedical Optics Express 4551
Biomedical Optics EXPRESS

Two-photon microperimetry: sensitivity of human photoreceptors to infrared light

Daniel Ruminski,[1,2,9] Grazyna Palczewska,[3,9] Maciej Nowakowski,[4] Agnieszka Zielińska,[2] Vladimir J. Kefalov,[5] Katarzyna Komar,[2,6] Krzysztof Palczewski,[1,7,10] and Maciej Wojtkowski[6,8,11]

[1]*Department of Pharmacology, School of Medicine, Case Western Reserve University, 2109 Adelbert Rd, Cleveland, OH 44106, USA*
[2]*Institute of Physics, Faculty of Physics, Astronomy and Informatics, Nicolaus Copernicus University in Torun, Grudziadzka 5, 87-100 Torun, Poland*
[3]*Polgenix, Inc., Department of Medical Devices, 5171 California Ave., Suite 150, Irvine, CA 92617, USA*
[4]*AM2M LLC LP, 7/17 Mickiewicza Street, 87-100 Torun, Poland*
[5]*Department of Ophthalmology and Visual Sciences, Washington University School of Medicine, 660 S. Euclid Avenue, Saint Louis, MO 63110, USA*
[6]*Baltic Institute of Technology, Al. Zwyciestwa 96/98, 81-451 Gdynia, Poland*
[7]*Gavin Herbert Eye Institute and the Department of Ophthalmology, University of California, 850 Health Sciences Road, Irvine, CA 92697, USA*
[8]*International Center for Translational Eye Research, Institute of Physical Chemistry, Polish Academy of Sciences, Kasprzaka Str. 44/52 01-224, Warsaw, Poland*
[9]*Equal contribution*
[10]*kpalczew@uci.edu*
[11]*mwojtkowski@ichf.edu.pl*

Abstract: Microperimetry is a subjective ophthalmologic test used to assess retinal function at various specific and focal locations of the visual field. Historically, visible light has been described as ranging from 400 to 720 nm. However, we previously demonstrated that infra-red light can initiate visual transduction in rod photoreceptors by a mechanism of two-photon absorption by visual pigments. Here we introduce a newly designed and constructed two-photon microperimeter. We provide for the first time evidence of the presence of a nonlinear process occurring in the human retina based on psychophysical tests using newly developed instrumentation. Since infra-red light penetrates the aged front of the eye better than visible light, it has the potential for improved functional diagnostics in patients with age-related visual disorders.

1. Introduction

Perimetry is a psychophysical method used to assess retinal function at various locations of the visual field and is an important component of ophthalmological practice [1]. This examination is used as a tool for detecting the progression and diagnosis of many eye diseases [2]. One perimetric technique, called microperimetry allows examiners to localize the position of the light stimulus applied to the retina and compare the visual function outcome with the underlying fundus image [3–6]. Microperimetry is an extension of classical perimetry used to localize the position of an applied stimulus by regular SLO. Therefore, it relates to the accuracy of localization rather than to the size of the target or to the extent of the visual field measured [1,7]. Further improvement of the localization was achieved by using Adaptive Optics techniques incorporated into Scanning Laser Ophthalmoscopy (AO-SLO). As it already has been demonstrated the combination of AO-SLO with an eye tracking system enables psychophysical studies to be performed on a cellular scale with microscopic precision [8–10].

#368129 https://doi.org/10.1364/BOE.10.004551
Journal © 2019 Received 22 May 2019; revised 16 Jul 2019; accepted 17 Jul 2019; published 9 Aug 2019

Biomedical Optics EXPRESS

Similar to standard perimetry, microperimetry permits the acquisition of information about the differential light sensitivity (DLS). DLS is the minimum luminance of a white-spot stimulus superimposed on a white background of uniform luminance. Recently, it has been reported that inconsistencies associated with microperimetry and the analysis of DLS limit conclusions regarding the use of microperimetry in the diagnosis of many eye diseases, especially in Age Related Macular Degeneration (AMD) [11].

The perception of infrared light through two-photon (2P) excitation of visual pigments was initially demonstrated in 2014 [12]. In this process, IR light activates retinal pigments through 2P absorptions that lead to photoisomerization of the chromophore, 11-*cis*-retinylidene, of both rod and cone pigments.

The human macula, about 5.5 mm in diameter, represents the cone-rich, center portion of the retina [13–16]. In this region, comprised of the fovea, parafovea and perifovea, age-related retinal degeneration such as AMD as well as juvenal forms of retinal degeneration such as Stargardt disease, take place [17]. In contrast, retinitis pigmentosa (RP), a genetically inherited progressive retinal degeneration occurs in the rod-rich peripheral section of the retina [18]. The ability to measure and map the retinal function of rods and cones at predefined regions of the retina is indispensable for identifying and monitoring the progression of retinal dystrophies as well as the impact of therapeutic interventions.

We assume that the perception of infrared light through two-photon (2P) excitation of visual pigments will improve the sensitivity of microperimetry when applied to aged eyes suffering from increased optical opacities. Near IR light is scattered less by the ocular media and is less affected by the aging process. Additionally, nonlinear optical processes like 2P excitation require delivering short pulses to well-defined regions of the outer segments of photoreceptors and therefore can be more precise in identifying dysfunctional retinal locations.

In this report, we introduce for the first time 2P microperimetry. This new method permits the measurement of IR light sensitivity in human subjects topologically as well as temporal changes in rod and cone dark adaptation. Notably, near infra-red light (IR) ranging from 700 to 1100 nm penetrates the aged front of the eye better than visible light, allowing improved simultaneous imaging and functional diagnostics in patients with age-related visual disorders. Furthermore, we designed a novel instrument for studying 2P vision in humans using a psychophysical method. By measuring visual sensitivity thresholds in dark- and light-adapted subjects, we establish for the first time that both cone and rod mediated human IR vision is triggered by 2P absorption. Moreover, psychometric functional studies indicated that visual sensitivity threshold measurements with visible light had a larger spread in comparison to measurements with IR. Finally, we demonstrated that visual function measurements with IR light are impacted less by lens opacities present in the aged eye, as compared to measurements with visible light.

2. Methods

2.1. 2P microperimeter

The system for measuring infrared (IR) and visible (VIS) light visual sensitivity (2PO-VIS) consisted of three modules (Fig. 1): a light delivery module producing the stimulating VIS and IR light beams, an SLO module generating an image preview of the fundus and a 2P microperimetry module enabling functional studies with IR and VIS light anywhere within the field of view of the SLO image. The imaging capacity of the system provides precise control of the retinal location of the sensitivity measurement through the real time SLO retinal preview. The IR light is generated by the HighQ-2 laser (Spectra-Physics, Santa Clara, CA) which delivers 250 fs-long pulses with a 1045 nm central wavelength and a repetition rate equal to 63 MHz. The VIS light at 522.5 nm is produced by diverting a portion of the IR beam (~94%) onto a non-linear crystal, BBO (OptoCity, Raleigh, NC). After BBO, the remaining IR light is routed onto a beam absorber.

Biomedical Optics EXPRESS

Both IR and VIS beams are coupled to a single-mode optical fiber (schematically shown as SF) that also enables spatial filtering of the stimulating beams.

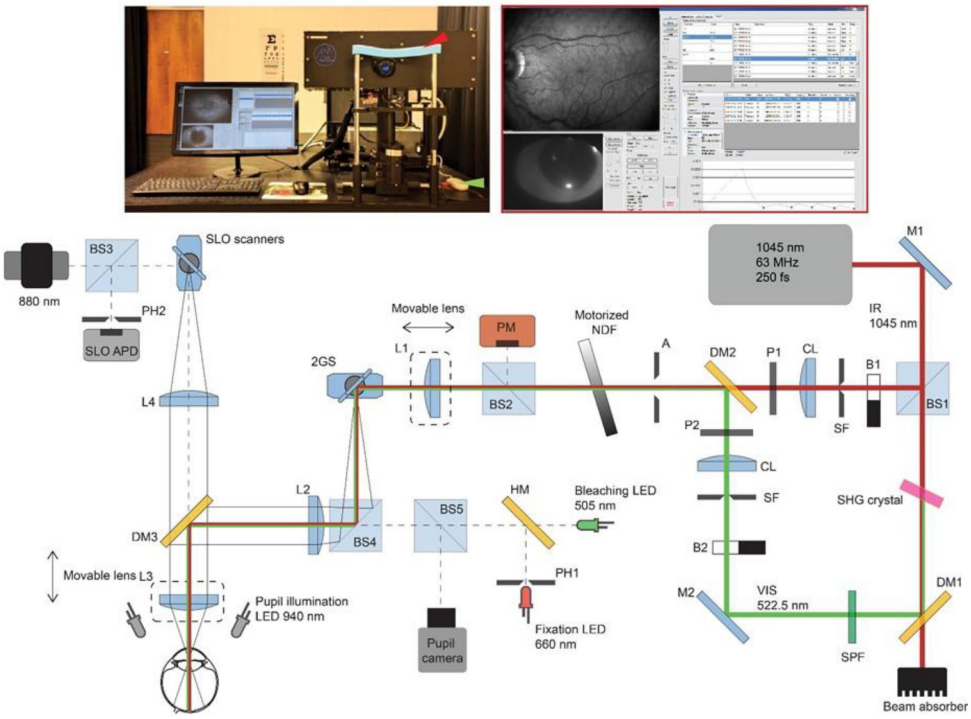

Fig. 1. System for measuring visual sensitivity to infrared and visible light (2PO-VIS). Photograph of the 2PO-VIS is shown in the upper left corner, the system control screen is shown in the upper right corner and the diagram of the system is shown in the central portion of the figure. In the photograph, the red arrowhead indicates the forehead rest and the green arrowhead indicates the computer mouse used to adjust the stimulus power. SLO preview and pupil image are displayed on the system control screen. The light delivery module (right portion of the system diagram) provides both stimulating wavelengths: 1045 nm (IR) and 522.5 nm (VIS) and is composed of a pulsing laser delivering 1045 nm light at 63 MHz; BS1 – a beam splitter uncoupling 15% of the beam; M1, M2 – flat mirrors; SHG – nonlinear crystal generating second harmonic light at 522.5 nm; DM1 – a long pass dichroic mirror; SPF – a short pass filter; B1, B2 – electronically controlled beam blockers; and two SF – optical fibers providing spatial filtering. The 2P microperimetry module enables functional studies with IR and VIS light anywhere within the field of view of the SLO image. The 2P microperimetry components consist of CL – collimating lenses; P1 and P2 – polarizers; DM2 – a long pass dichroic mirror; A – an adjustable aperture; motorized NDF – a gradient neutral density filter; BS2, BS4, BS5 –beam splitters; PM – a power meter; L1 – movable lens correcting for refraction error; movable lens L3; 2GS –2D galvanometer scanners; L2 and L3 – telescopic system conjugating the pupil plane with scanners 2GS; DM3 – a dichroic mirror coupling the SLO beam with stimulating beams; HM – a hot mirror; PH1 - pinhole. The SLO imaging components include BS3 – beam splitter; SLO scanners – a resonant scanner and a galvanometer scanner; lenses L4 and L3 – telescopic system conjugating the pupil plane with scanning stage and enabling SLO field of view in a range of $30° \times 24°$ at the retinal plane; PH2 – a pinhole; APD – an avalanche photodiode. Solid black lines outline extreme scanning beam paths for IR, VIS, and SLO beams.

Biomedical Optics EXPRESS

For the SLO imaging, an 880 nm light beam from an LP880-SF3 diode (Thorlabs, Newton, NJ) is sent to the scanner module consisting of a resonant scanner (4 kHz, Cambridge Technology, Bedford, MA), operating in the Y direction, and galvanometer scanner (Thorlabs). This configuration enables SLO imaging with 9.4 frames per second for images with a size of 800 lines × 600 pixels. The detection optical system of the SLO module consists of a focusing lens (omitted in Fig. 1), a 105 μm diameter confocal pinhole (PH2) and an avalanche photodiode (SLO APD). Considering the eye's pupil diameter (D = 7 mm), geometry of the returning beam (given by the 4f system telescope, lenses: L3, L4 in Fig. 1), the clear aperture of the scanning system (9 mm), and focusing lens parameters (f = 30 mm, 0.15 NA with 9 mm diameter beam), the Airy disc diameter of the detection path equals about 7 μm. Thus, our detection pinhole size normalized in respect to the Airy disc diameter equals about 15 (confocal pinhole diameterPH2/Airy disc diameter) [19]. Such a large value for the detection confocal pinhole comes from the system design needed for high light collection efficiency. The SLO module works with a very low illumination beam power (70 μW, collimated beam at the cornea) in order not to affect the visual experience of subjects, so in this instance the resolution of the SLO system was sacrificed. The lens L3 is mounted on a motorized stage to correct the refraction error of a subject's eye. The diameter of the SLO beam on the cornea is equal to 2 mm ($1/e^2$). Optical arrangement of an imaging telescope composed of lenses L4 and L3 provides an SLO field of view of 30° × 24° at the retinal plane.

In the 2PO-VIS system, the 522.5 nm (VIS) and 1045 nm (IR) beams are coupled together into one optical path by a long pass dichroic mirror (DM2). The selection of either VIS or IR is accomplished with electronically controlled beam blockers (B1, B2). Two collimators (CL) are set to compensate for the differences of longitudinal chromatic aberrations (LCA) of the human eye and the system between two stimulating wavelengths, IR and VIS. The polarization states of both stimulating beams are controlled by polarizers, P1 (LPNIRE100-B, Thorlabs) and P2 (LPVISE100-A, Thorlabs). The adjustable aperture A, placed in the plane conjugated to the galvanometer scanners and the eye's entrance pupil plane, allows changes to the size of the stimulating beam entering the subject's eye. Both beams travel through a motorized gradient neutral density filter (NDF) with a position controlled by the subject during psychophysical studies. A portion of the stimulating beam (~50%) is directed onto the power meter (PM) by a beam splitter (BS2). Thus, the light power delivered to the eye is constantly monitored through calibrated readings of a PM. An additional attenuating filter (not shown) is placed into the optical path between BS2 and the stage of the galvanometer scanners (2GS) attenuating the VIS beam to ensure that a very low power (a fraction of a pW) reaches the subject's cornea. The optical plane of the pair of galvanometer scanners (2GS) is conjugated to the eye pupil plane by a telescope consisting of lenses L2 and L3. The dichroic mirror DM3 (DMSP1000R, Thorlabs), placed in the common focal plane of these two lenses, combines the optical paths of the SLO and 2P microperimetry modules that both operate simultaneously. The diameters of the stimulating VIS and IR beams on the cornea are equal to 1.5 mm ($1/e^2$). Stimulating beams are focused on the retina by the optics of the subject's eye and are scanned on the retina with at 100 Hz frame rate. The stimulus pattern is displayed on the retina intermittently for 0.2 s every 0.6-0.8 s.

Bleaching is performed with a 505 nm light emitting diode (LED) or white light illuminating the retina in a Maxwellian view arrangement. The fixation spot is formed by light emitted by a 630 nm LED passing through a pinhole, PH1. Additional lens arrangements (not shown), together with the L2 lens form an image of the fixation point on the surface of DM3, optically conjugated with the retinal plane. A hot mirror (HM) (FM02R, Thorlabs) couples both fixation and bleaching light beams into one optical path. Such an optical arrangement ensures uniform illumination of the subject's retina by the bleaching light. A beam splitter, BS4, combines light from the LED sources and stimulating IR and VIS light. The pupil of a tested eye is illuminated by a 940 nm LED and the image is registered by a pupil camera.

Biomedical Optics EXPRESS

The system correcting refractive error includes global correction - implemented with the movable lens L3 (Fig. 1), which is the main refractive error correcting element for the SLO imaging module but also provides a coarse correction for the VIS/IR beam and the fixation channel. In order to further refine the refraction correction tuning for the VIS beam and IR beam the movable lens L1 is used. The fine tuning for the fixation channel is provided by changing the position of the fixation target's object plane.

2.2. Visual sensitivity threshold measurements

Psychophysical tests were performed either in dark or light adapted conditions. Scotopic (E^S) and photopic (E^V) illuminances were measured with a MSC15 Spectral Lightmeter (Gigahertz-Optik, Turkenfeld, Germany) placed at a distance d = 52 mm after the focal plane of L3 (Fig. 1). Scotopic or photopic retinal illuminances ($E_R{}^{S/V}$), and the fraction of bleached rhodopsin (B) were calculated according to Thomas et al. [20]. In brief, the retinal illuminances, scotopic $E_R{}^S$ or photopic $E_R{}^V$, expressed in trolands (Td) could be calculated from the approximate expression $E_R{}^{S/V} \approx E^{S/V} \cdot d$, where d stands for the distance between the Lightmeter and the focal plane of L3. Then, the formula to calculate the bleached fraction of rhodopsin, B, can be expressed as $B = 1 - \exp(-L/L_{Rh})$, where $L = E_R{}^S \cdot t$ is the time integrated scotopic retinal illuminance, L_{Rh} is the 'bleaching constant' equal to 10^7 Td · s. During experiments with light adaptation measurements, IR and VIS stimuli were displayed on the subject's retina with an increasing photopic retinal illuminance background up to 1.8×10^3 Td. To perform dark-adaptation tests subjects stayed in darkness for 30 min. During the measurements, the IR or VIS stimulus in the form of a 0.4° diameter, re-scanned circle was displayed on the subject's retina. Subjects were asked to adjust the beam power, to reach a visibility threshold, with an optical mouse scroll that regulates the position of the motorized gradient neutral density filter (NDF in Fig. 1). Once the visibility threshold was reached, the subject was asked to click the mouse button. The threshold power of the stimulating beam was recorded by an internal power meter (PM in Fig. 1) and simultaneously, the SLO image was captured, thereby recording the position of the stimulus on subject's retina. After recording the visibility threshold, the stimulus power was automatically increased to reach a level 3-fold higher than the just recorded threshold value. This procedure was repeated up to five times. Automatic power increase (3-fold) after every threshold record was chosen arbitrarily in order to ensure similar conditions for every sample within the test: the subject then adjusted the bright stimuli power until a threshold power was reached.

To evaluate psychometric function, measurements of the detection frequency were done by displaying stimuli at various powers on a subject's retina, and the subject's task was to click the left mouse button when the stimulus was detected and the right button when it was not detected. The stimuli were displayed on the central retina on a green, 505 nm, 86 Td (photopic units) background. Stimuli powers graded into 9 bins were displayed repeatedly and randomly around the central power T_{seedIR} for IR and $T_{seedVIS}$ for VIS, found using methods of adjustments [21]. To achieve similar sampling density around T_{seed}, we chose different power intervals for VIS and IR. IR stimulus power in linear scale was graded into $0.07 \cdot T_{seedIR}$ intervals and for the VIS stimulus we chose $0.12 \cdot T_{seedVIS}$ intervals around their corresponding T_{seed}. Probability of stimuli detection can be described by logistic distribution p(x) [22,23]

$$p(x) = 1/(1 + \exp[(T - x)/\sigma]), \tag{1}$$

where x is stimuli power; T represents the threshold power for which stimuli were seen with p(T) = 0.5; and σ is a constant, that corresponds to the function spread. Data and p(x) were plotted as a function of stimuli power in decibel scale, normalized to corresponding IR and VIS thresholds (T).

For the assessment of the repeatability, the same subject's eye was measured in two sessions, test 1 and test 2, separated by 2 h. In each test, five consecutive measurements were collected

Biomedical Optics EXPRESS

with both IR and VIS light. The stimulus was displayed on the central retina on a green, 505 nm, 485 Td (photopic units) background. The sensitivity (S) was calculated as the inverse of the average threshold power from five measurements, S = 1/(threshold power) and converted to a decibel (dB) scale using 100 pW of threshold power as the reference value. This reference was chosen arbitrarily as the maximum power of VIS beam that could be generated by our device. The brightness of such a stimulus was easily visible to every participant of the study. Moreover, we treated this value as a single reference for both stimuli to enable easy comparison between their powers. Data were evaluated by Bland-Altman analyses [24,25]. Thus, each subject was indicated as a point on the XY Bland-Altman plot, where the X-axis represented mean values from the two tests, and the Y-axis represented the difference between the averages of two tests (Log ($S_{test\ 1}$) − Log ($S_{test\ 2}$)). Standard deviations of the differences (SDD) for IR and VIS were calculated to assess the repeatability of each method. The 95% limits of the repeatability corresponded to the interval −1.96·SDD to 1.96·SDD.

During long-term dark adaptation measurements, performed by using a laboratory system in NCU, Torun (Fig. 2), the position and size of the subject's pupil were monitored by using an infrared camera. Furthermore, IR and VIS visual sensitivity thresholds were measured with 3°20' stimuli without additional retinal illuminance, at various time intervals after exposing the retina to uniform light.

The stimulus delivery module at NCU Torun was basically the same as the light path for the stimulus of the perimeter shown in Fig. 1. The light sources were: 1040 nm laser delivering 250 fs pulses at a repetition rate of 76 MHz and its second harmonic at 520 nm. Both beams have been coupled to single mode fibers of 5 m length. Collimated beams from fiber outputs were coupled together by using a dichroic long pass mirror and after passing throughout the regulated aperture as well as the telescope consisting of two lenses, both of f = 50 mm, they were reflected by a pair of galvanometric scanners. Before the scanners, portions of the beams were uncoupled by a 50:50 beamsplitter to the power meter sensor. Next, scanner beams were routed through the second telescope consisting of 75 mm and 50 mm lenses (already shown in Fig. 2(a)).

2.3. Assessment of light opacities influencing NIR stimulation

To assess the impact of light opacities on IR and VIS visual sensitivity, donor human eye lenses or an artificial diffuser were placed in the optical path of the 2PO-VIS after L3, and IR and VIS sensitivity or intensity profiles were measured. The stimulating beam at the plane of the lenses or artificial diffusor was collimated, therefore light transmittance was affected within 1.5 mm ($1/e^2$) of the stimuli beam size. Intensity profiles were measured at the focusing plane of a Bi-Convex, f = 25.4 mm lens, placed after L3, using a beam profiling camera, WinCamD-LCM (DataRay Inc., Redding, CA). The artificial diffuser was prepared by filling a disposable cuvette with clear RTV silicone #80050 (Permatex, division of ITW, Solon, OH), cured at ambient room temperature (20–22 °C) for 72 h.

Transmittance spectra were measured with a spectrometer, Lambda BIO+ (PerkinElmer, Waltham, MA) following a standard procedure and using a cuvette filled with PBS (phosphate buffered saline solution composed of 9.5 mM sodium phosphate, 137 mM NaCl, and 2.7 mM KCl, pH 7.4) as a reference. Pulse durations were measured with the use of an autocorrelator (Carpe, APE GmbH, Germany).

Two dimensional maps and 3D representations of sensitivity distribution were assembled from visual sensitivity threshold data points at 45 different macular locations around the fovea. During these measurements, SLO retinal preview was used to control the eye position. While a subject was asked to focus their gaze on the fixation light and find the visibility threshold to IR and VIS light, different areas around the fovea were probed with IR and VIS light. Two-dimensional sensitivity maps and 3D representations were derived from measurement points using linear

Biomedical Optics EXPRESS

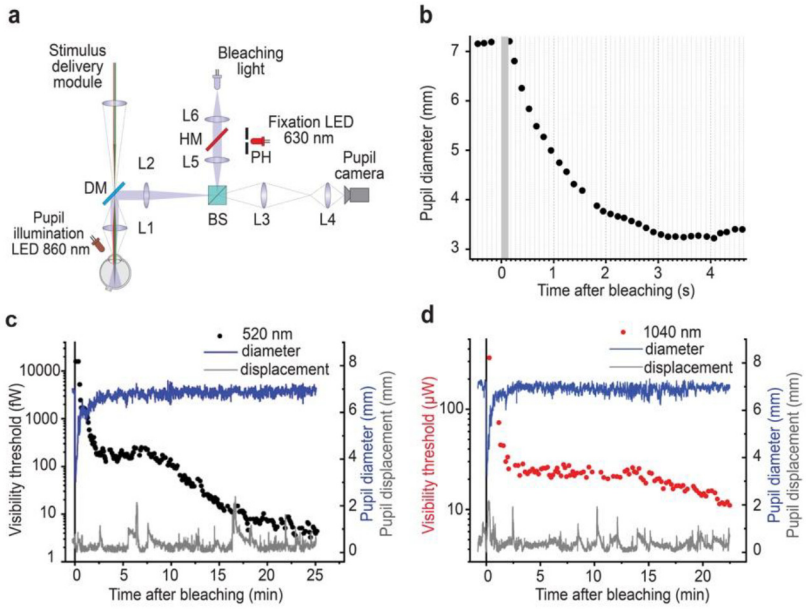

Fig. 2. System for simultaneously monitoring dark adaption, pupil diameter and pupil position. (a) Scheme of the part of the optical system in NCU Torun for psychophysical measurements dedicated to monitoring the pupil and bleaching light delivery. Pupil monitoring optical path consisted of two telescopes, first, lenses L1 and L2 and the second, lenses of L3 and L4, USB CMOS camera, dichroic mirror DM for coupling stimulus light with pupil illumination and beamsplitter BS for coupling bleaching and fixation. The 860 nm light from LED diodes was used for pupil illumination. Stimulus delivery module is not shown. The bleaching source was a white LED and the two telescopes (L1 and L2; L5 and L6) formed the image of the LED at the pupil providing uniform illumination at the retinal plane. Hot mirror HM coupled 630 nm light for fixation with the optical path of bleaching. The 100 μm pinhole PH placed in the plane conjugated to the retina, formed a point-like source for fixation. (b) Changes of pupil size over time during the first few seconds of dark adaptation measurements after bleaching. The gray stripe corresponds to a bleaching event lasting 150 ms. Changes in pupil displacement, gray line, and diameter, blue line, during dark adaptation measurements: (c) trial with VIS stimulus: black dots - transient visibility threshold for 520 nm; (d) trial with IR stimulus: red dots - transient visibility threshold for 1040 nm.

interpolation and smoothing with a two-dimensional Gaussian kernel in the Python SciPy library and visualized using Matplotlib [26].

2.4. Human subjects

Subjects were comprised of 17 volunteers between 26 and 65 years of age. No clinical ophthalmic exams were done. Subjects did not stipulate to any visual problems. Refraction errors were compensated as described in methods.

The study with human volunteers was approved by the University Hospitals Cleveland Medical Center, University Hospitals Institutional Review Board (IRB), and the Ethical Committee Collegium Medicum in Bydgoszcz, Nicolaus Copernicus University (NCU) in Torun, Poland. It conformed to the World Medical Association Declaration of Helsinki: Ethical Principles for Medical Research Involving Human Subjects [27]. Signed informed consents were obtained

Biomedical Optics EXPRESS

from all subjects before starting the procedures. All tests were conducted in compliance with the American National Standard Institute (ANSI Z136.1-2014).

Although we stimulated the retina using a scanning laser beam, the calculations below are provided for a static one, which gives a more restrictive maximum permissible exposure (MPE) value and can be applied even for the smallest optotypes. We also assume an immobilized eye, due to using a chinrest and fixation. We have used long exposures of the retina, one measurement of dark adaptation lasted up to 30 minutes, so to provide a safety margin, we performed a calculation for 60 min and a light source providing 250 fs at the laser output and elongated by the fibers of different length up to 10 ps, with repetition frequency 63 MHz (76 MHz in NCU) and wavelength 1045 nm (1040 nm in NCU). Based on paragraph 8.2.3 and Table 1 of ANSI Z136.1-2014, for calculating MPE for repetitive-pulse exposure, in the case of both lasers used in this study and for all pulse lengths applied, the most restrictive would be Rule 2 (Average Power). Wavelength-dependent parameter CA was calculated according to ANSI Table 6(a) and was equal to 4.9 for 1045 nm and 4.8 for 1040 nm. MPE for a group of pulses according to Table 5(c) of ANSI is then equal to:

$$MPE = (1.8 \cdot 4.9 \cdot 3600^{0.75} \cdot 10^{-3})\frac{J}{cm^2} = 4.1\frac{J}{cm^2} \tag{2}$$

for 1-hour exposure of an immobilized eye for a 1045 nm laser. Dividing the above by exposure time, t = 3600 s, and multiplying by the pupil area, 0.385 cm^2, we obtained corresponding maximum permissible power P_{max} value at the cornea for 1045 nm laser:

$$P_{\max} = MPE\left[\frac{mJ}{cm^2}\right] \cdot t^{-1}[s^{-1}] \cdot 0.385 cm^2 = 0.438 mW. \tag{3}$$

The same calculations for the laser at NCU: MPE = 4 J/cm^{-2} and P_{max} = 0.428 mW.

Subjects were asked to place their chins and foreheads on a forehead-chin rest holder. A fixation target was displayed to facilitate eye stabilization during the tests. Raw adjustment of a subject's eye position was obtained by using feedback from a pupil camera preview, while fine adjustment was achieved with a scanning laser ophthalmoscope (SLO) retinal preview.

3. Results

3.1. Two vs one-photon absorption

Our new instrumentation permits the stimulation of the retina with two light beams: 1040 nm and 520 nm, that both were perceived as green by all investigated subjects.

To initially verify that the IR channel delivers retinal stimulation related to 2P absorption we measured visual sensitivity thresholds to IR and VIS light as a function of pulse duration. Pulse duration was modified by increasing the dispersion of our system with the use of variable-length optical fibers inserted in locations between P1 and B1 for IR and P2 and B2 for VIS (Fig. 1). With the use of an autocorrelator, we estimated that after increasing fiber length from 1 m to 38 m, pulse duration increased from 490 fs to ~10 ps (~20 fold). In parallel, IR visual sensitivity threshold also increased (~3.6 fold), whereas the VIS visual sensitivity threshold remained unchanged (Fig. 3(a)). With pulsing laser stimuli, the number of 2P absorptions is proportional to the square of the average power of the laser beam and inversely proportional to the pulse duration [28]. Assuming the same number of 2P absorptions need to occur for the same visual sensation, we expected a 4.5-fold increase in the IR visual sensitivity threshold. Thus, we verified, with our upgraded system, the earlier finding that IR vision is initiated by 2P absorption.

3.2. Light adaptation

Considering that one-photon (1P) absorption is proportional to light intensity and that 2P absorption is proportional to the square of light intensity, we measured IR and VIS visual

Biomedical Optics EXPRESS

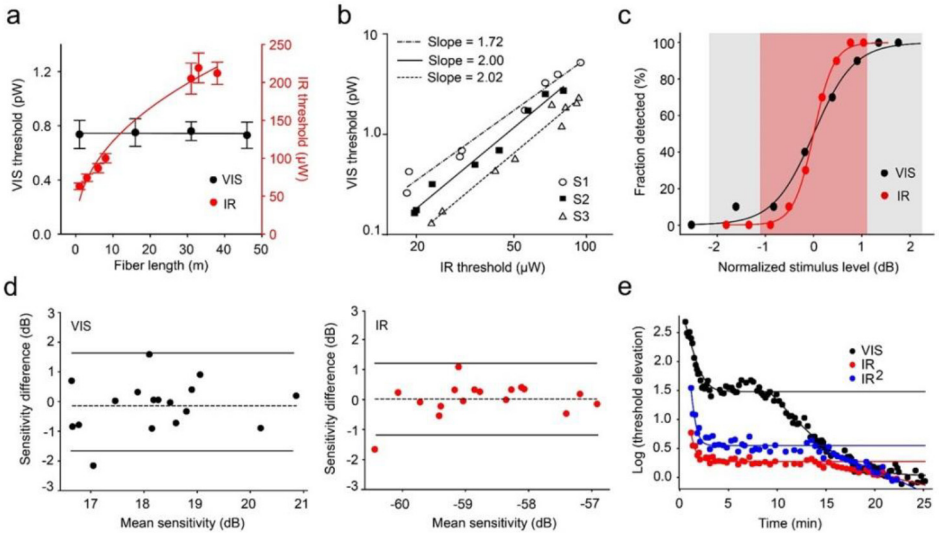

Fig. 3. Measurements of visual sensitivity to IR and VIS light. (a) The IR (red circles) but not VIS (black circles) visual sensitivity threshold is impacted by increased dispersion introduced by variable lengths of the optical fiber. Measurements were performed in the fovea. Line drawn through IR data points is described by equation VIS threshold = 44 × (IR threshold)$^{0.44}$. Error bars represent standard deviations, n = 5. (b) Log-log plot of the VIS light sensitivity thresholds as a function of IR light sensitivity thresholds obtained in three volunteer subjects S1 (48-year-old), S2 (61-year-old), and S3 (32-year-old). Points on a 2D plot represent pairs of VIS and IR thresholds collected with the same retinal luminance background, which ranged from 0 to 1.8×10^3 photopic trolands. Lines through the data points were obtained with the linear regression fit, and their slopes are indicated. (c) Psychometric function. The X axis values are normalized to the threshold power at which the stimulating pattern, VIS or IR, was seen in 50% of trials. The 99.7% of the change in psychometric function value occurred within ± 1.1 dB range for IR, indicated as solid red background, and within ± 2.2 dB for VIS [23], indicated as solid gray background. Black and red circles indicate experimental data points corresponding to VIS and IR data, respectively; solid black and red lines represent logistic distribution obtained for VIS and IR accordingly [23]. (d) Bland-Altman analysis of sensitivity measurements repeatability. Each of 17 subjects is indicated as a point on a 2D plot, with the abscissa representing the average sensitivity value and ordinate representing the sensitivity difference between two tests. Data obtained with VIS stimuli are shown as black dots and data obtained with IR are shown as red dots. Dashed lines correspond to the overall mean sensitivity difference between the two tests. Solid lines were calculated as described previously [24,25] and outline the limits within which 95% of the intra-session sensitivity differences are expected to fall. (e) IR and VIS dark adaptation. The data were obtained with the laboratory apparatus at Nicolaus Copernicus University in Torun (NCU), using a white light emitting diode for bleaching, 630 nm fixation light, and pupil camera with 860 nm central wavelength. Shown are visual sensitivity thresholds measured after bleaching with 7.3×10^6 Td·s (scotopic units). Visual sensitivity thresholds were measured in the right eye of a 40-year-old subject, at the location 6°30' temporal from the fovea using an empty circle stimulus with the diameter 3°20'. Black and red circles represent data points obtained with VIS and IR respectively. Blue circles represent IR data squared. Plots are normalized to pre-bleached sensitivity threshold values.

Biomedical Optics EXPRESS

sensitivity thresholds on the same, however, variable photopic retinal illuminance background in three subjects. Assuming, as before, that the same number of isomerization events is needed to occur via 2P and 1P processes to initiate visual sensation, we expected a square relationship between VIS and IR visual sensitivity thresholds measured at the same retinal location. To quantify this process, we modulated the sensitivity thresholds by applying a variable photopic retinal illuminance background. For each retinal illuminance background VIS visual sensitivity thresholds were plotted on a log-log plot as a function of IR visual sensitivity threshold for 3 subjects (Fig. 3(b)). For the three subjects the slope was within the range 1.7–2 in log scale corresponding closely to a square ratio, confirming that IR visual sensitivity thresholds are obeying a nonlinear process. These data provide the first direct evidence of nonlinear stimulation of photoreceptors in human subjects by IR. Subjects S1 and S2 required more VIS light than subject S3 to attain a visual sensitivity threshold, perhaps indicating light opacities in their anterior segment of the eye. These data provide the first direct evidence of nonlinear stimulation of photoreceptors in human subjects by IR.

3.3. Psychometric function

To understand better the accuracy of determining the visual sensitivity thresholds for VIS and IR light, we measured a psychometric function in response to stimuli with variable power. This function plays a basic role in psychophysics, as it describes the probability of a particular psychophysical response as a function of the stimulus strength depending on the frequency of the yes/no responses [22,29].

This function is analytically described by logistic distribution, see Eq. 1 in Methods, and had a larger spread, σ=0.42 for VIS light in comparison to IR light, σ=0.21 (Fig. 3(c)). Threshold values (T) representing stimuli powers for which probabilities of detecting stimuli p(T) were equal to 0.5 were derived from distribution fits and were equal to 480 fW for VIS light and 73 µW for IR light. In both cases the R^2 parameters of our fits were greater than 0.99. Results presented in Fig. 5(c) were normalized to corresponding T values to compare relative differences between IR and VIS stimuli. The 99.7% of the change in the psychometric function value occurred within the ± 1.1 dB range for IR light, indicated as a solid red band in Fig. 3(c), however for VIS light this range was larger, ± 2.2 dB [23], indicated as a solid gray background in Fig. 3(c).

The calculated psychometric function for infra-red retinal stimulation is two times narrower than that calculated for standard stimulation using visible light. According to results presented in Section 3.2, VIS sensitivity threshold power is proportional to IR sensitivity threshold power squared: VIS~IR^2. Considering this relation, Eq. 1 can be modified:

$$p[\log(x^2)] = (1 + \exp[(\log(T^2) - \log(x^2))/\sigma])^{-1} = (1 + \exp[\log(T/x)/(0.5 \cdot \sigma)])^{-1}. \quad (4)$$

Therefore, the psychometric function when represented in logarithmic scale results in halving the function spread.

3.4. Repeatability of the measurements, Bland-Altman analysis

To compare the repeatability of sensitivity measurements between IR and VIS stimulation we measured visual sensitivity thresholds in two sessions in each of 17 subjects (Fig. 3(d)). Subjects were between 26 and 60 years of age (average age (and SD) of the subjects was 38.7 ± 10.5 years). Mean sensitivity from two sessions for all subjects varied from 16.6 dB to 20.9 dB, and the average sensitivity difference between the two sessions across all subjects was −0.15 dB for the VIS group. For the IR light, mean sensitivity from two sessions for all subjects varied from −60.4 dB to −56.9 dB, and the average sensitivity difference between the two sessions across all subjects was 0.02 dB. Thus, there were no systematic differences between the two sessions for both stimuli. Standard deviations of the differences (SDD) were 0.58 dB and 0.87 dB for IR and VIS respectively. Moreover, the 95% limits of the repeatability equaled 1.7 dB and 1.1 dB for

Biomedical Optics EXPRESS

VIS and IR accordingly. These results indicate that visual sensitivity threshold measurements with IR light had better repeatability in comparison to VIS light.

3.5. Dark adaptation

To compare rod and cone responses to IR and VIS stimuli, we measured visual sensitivity threshold recovery after brief exposure to white light (Fig. 3(e)) for a healthy subject (40-year old). IR and VIS visual sensitivity thresholds in response to 3°20' stimuli located in the parafovea, centered at 6°30' temporally were measured at various time intervals after exposure to $7.3{\cdot}10^6$ Td·s (scotopic units) of white LED light, corresponding to 52% bleached rhodopsin [20]. Plots were normalized to pre-bleached sensitivity threshold values expressed as mean power in Watts at the pupil plane and represented in logarithmic scale, as seen in Fig. 3(e). Plots have a classical bi-phasic form of threshold recovery [30]. VIS and IR cone recoveries rapidly reached plateaus at 1.5 log and 0.3 log respectively. After the cone-rod break, the recovery was dominated by the rod dark adaptation. The cone-rod break occurred at ~10 min for VIS and at ~15 min for the IR test. Moreover, the late rod recovery portion of the dark adaptation curve for the VIS stimulus coincided with the curve for the IR stimulus for the squared stimuli. Plateaus for each of the recovery phases were at 154 fW (cones) and 5.4 fW (rods) for VIS stimulation, and 23.4 μW (cones) and 12.4 μW (rods) for IR stimulation. The increase in IR sensitivity threshold as compared to VIS sensitivity threshold was 1.2 log units smaller for cones than for rods. Thus, cone plateau was relatively longer for IR in comparison to the VIS plot in the dark adaptation experiment, perhaps enabling an expanded study of cone function. Full recovery was observed within 25 min for both stimuli. Furthermore, during dark adaptation measurements, subject's pupil size and position, were measured with the set-up shown in Fig. 2. The mean pupil diameter (except for bleaching) was similar and stable during VIS and IR measurements: 6.87 mm ± 0.14 mm for VIS stimulus and 6.93 mm ± 0.15 mm for IR. The pupil was slightly bigger, 0.06 mm, for the IR stimulus, possibly because scattered IR was not perceived by the human eye resulting in darker background for measurements with the IR stimulus compared with the VIS stimulus. The mean pupil displacement for the visible stimulus was 0.39 mm ± 0.23 mm, and for infrared it was 0.46 mm ± 0.25 mm demonstrating that the subject's eye was stable during the 25 min period of measurements.

3.6. Impact of lens opacities on VIS and IR visual sensitivity thresholds

Because the transmittance of the human lens deteriorates with age [31], we evaluated if using IR light can be beneficial to test visual function in older patients with lens opacities (Fig. 4). We found that after placing a diffuser consisting of a human lens from a 64-year-old donor in the light path between the 2PO-VIS instrument (Fig. 1) and a 32-year-old subject eye, visual sensitivity threshold increased 77 times for VIS light but only 29 times for IR light, thus the VIS sensitivity threshold increased 2.7 times more than the IR sensitivity threshold. When using a human lens from 45-year-old donor in a similar fashion, the VIS sensitivity threshold increased 2.3 times more than the IR sensitivity (Fig. 4(a)). The larger increase of VIS sensitivity threshold as compared to IR sensitivity threshold when using the lens from the older donor was supported by the % direct transmittance measurements as a function of wavelength of lenses from human donors (Fig. 4(b)). To mimic the impact of lens opacities on light scattering, and thus the smearing of light patterns, we generated a light pattern consisting of six evenly spaced lines and measured that pattern with the beam profiling camera. Without a diffuser both VIS (Fig. 4(c)) and IR (Fig. 4(d)) light beams clearly reproduced the pattern on the camera. However, after an artificial diffuser (RTV), having transmittance corresponding closely to that of natural lenses (Fig. 4(b)) was inserted in the light path, only the pattern generated by IR light was reproduced on the detector. In both cases, the integrating camera captures VIS as well as IR light during a 1-photon absorption process, so the figure does not truly compare 1-photon and 2-photon vision.

Biomedical Optics EXPRESS

However, using this simple test one can see that image structure already was lost for VIS light, while still maintained for IR light, which is very important for stimuli delivery during sensitivity testing. Cumulatively, these results demonstrate the advantage of using IR light when measuring retinal function in the aging eye or eyes with lens opacities, due to better penetration.

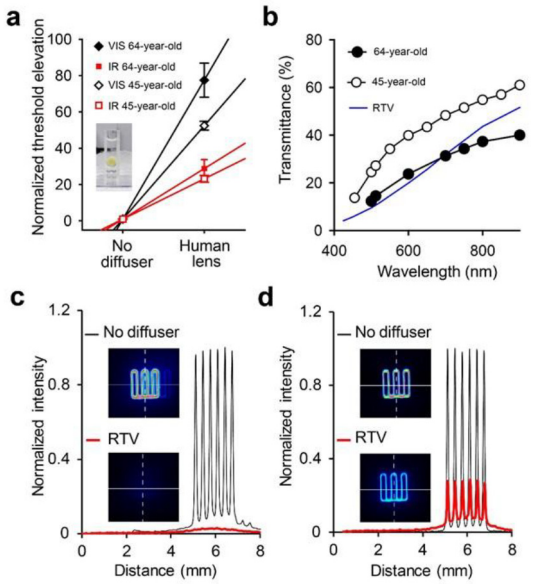

Fig. 4. Stimulation with infrared (IR) light is impacted less than stimulation with visible light (VIS) by human eye light opacities. (a) VIS (black) and IR (red) light visual sensitivity thresholds measured in a 33-year old subject with and without diffusers are shown. Diffuser consisted of a human donor lens submerged in PBS in a quartz cuvette as shown in the inset. Filled symbols represent data obtained with the lens from a 64-year-old human donor, and unfilled symbols correspond to the lens from a 45-year old human donor. Plots were normalized by dividing the visual sensitivity threshold value, by the average sensitivity value measured without a diffuser for VIS and for IR. Error bars represent standard deviations, n = 4. (b) Shown are transmittance spectra from the 64-year old human donor lens (filled black circles), 45-year-old human donor lens (unfilled circles) and the RTV diffuser (blue line). (c-d) VIS (c) and IR (d) light intensity profiles were measured with a beam profiling camera system without and with RTV diffuser. Both: VIS and IR stimuli consisted of six vertical lines separated by 0.32 mm. VIS light stimuli were at 70 nW and IR stimuli 20 nW. Upper row insets show color scale images of beam profiles obtained without a diffuser, and images obtained with a diffuser are shown in the lower row.

3.7. Macular sensitivity mapping

The spatial distribution of macular sensitivity was tested under scotopic conditions using both IR and VIS stimuli (Fig. 5). A healthy volunteer (32 yr) was dark adapted for 30 min and tested using the 2PO-VIS system. Forty-five different macular positions were probed to find local sensitivity values. Scanning laser ophthalmoscopy (SLO) retinal preview was used to control the position of the eye during the experiment (Fig. 5(a)). While the subject was asked to focus their gaze at the fixation spot, different areas around the fovea were probed (each position was probed once) and the subject was asked each time to determine the threshold light power. The sensitivity data points were spatially interpolated to create two-dimensional sensitivity maps (Fig. 5(b)). Three-dimensional visualizations of the infrared and visible light testing are shown in Fig. 5(c).

Biomedical Optics EXPRESS

As expected, the highest visual sensitivities, for both IR and VIS, were at the rod-dominant locations furthest from the fovea, and the lowest visual sensitivity was at the cone-rich fovea. It is also visible that a difference in sensitivity between the central fovea (with a higher concentration of cones) and its surroundings (with more rods) for visible light is larger (14 dB) than for infrared light (5 dB), which is consistent with results obtained for dark adaptation recovery (Fig. 5(e)). Data were normalized to the same reference power so that relative sensitivity differences could be assessed. IR sensitivity in the fovea was approximately 86 dB less than VIS sensitivity.

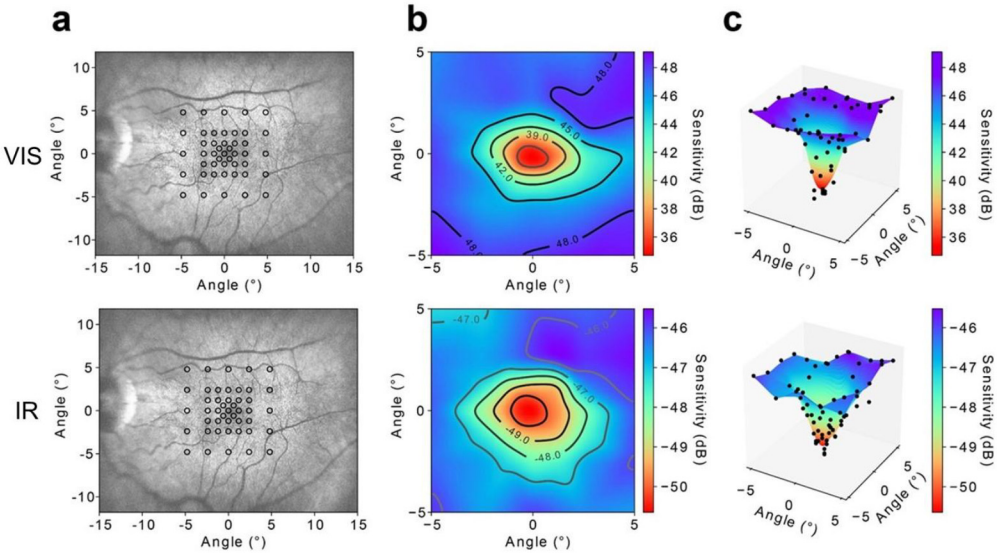

Fig. 5. Retinal maps of visual sensitivity thresholds to VIS and IR light. In all panels, data obtained with VIS are presented in the upper row and with IR in the lower row. (a) SLO retinal preview with an overlay of the 45 macular positions probed with the VIS and the IR light. (b) Contour maps of visual sensitivity. Sensitivity isolines overlaid on the maps are drawn with the 3-dB step for VIS and 1 dB for IR. (c) Three-dimensional representation of visual sensitivity centered on subject's fovea. Black points represent the measurement results and overlaid surfaces represent results of the interpolation. Macular sensitivity mapping was performed on a 32-year old subject.

4. Discussion

Although 1P and 2P vision can result in almost identical vision sensations, i.e. green light perception during stimulation with either short pulses of IR at 1045 nm or 523 nm light, there are advantages for choosing an IR stimulus for microperimetry testing. Infra-red light is less absorbed and less scattered in the eye in comparison to visible light. Experimental data from bovine eyes together with Monte Carlo simulation revealed that IR has better performance in all tested eye compartments [32]. Specifically, in the retina the photon mean free path was ~2 times longer at 1045 nm as compared with 523 nm. Furthermore, direct transmittances of the human lens and cornea at 523 nm decrease with age. For example, direct transmittance of the lens from a 75-year old donor is only ~30% of that from a 4.5-year-old donor; in contrast at 1045 nm, direct transmittance of the lens from a 75-year old donor is ~75% of that from a 4.5-year-old donor [31]. Moreover, VIS light is perceived by 1P vision, producing retinal stimulation by photons arriving at focus and out-of-focus, as well as internally reflected from other locations in the eye. Because of the presence of eye opacities in the anterior segment of the eye, the number of out-of-focus photons can be substantial, resulting in blurred stimuli patterns on the

Biomedical Optics EXPRESS

retina. In contrast, in the case of 2P vision, the retina is stimulated near the focal plane, where the photon flux is highest. The intensities of scattered and out-of-focus IR light are too small to induce 2P or 1P isomerization of visual pigments, resulting in smaller spread of IR visual sensitivity measurements in comparison to measurements with VIS light. Precise stimulation of individual foveal cone photoreceptors with VIS light at 543 nm can also be achieved with advanced optical instrumentation involving Adaptive Optics Scanning Laser Ophthalmoscopy (AO-SLO) and a cascade of acousto-optics modulators [33]. Currently, this method represents an excellent research tool, and also holds great potential for future routine testing of patients. Future combination of AO-SLO together with our 2P microperimetery potentially could improve stimuli delivery localization.

With a newly designed and constructed instrument for studying 2P vision we performed psychophysical tests of visual sensitivity thresholds and dark adaptation in selected retinal locations in response to IR and VIS stimuli. Both beams, i.e. IR at 1045 nm and visible light at 523 nm were perceived as green. Furthermore, by measuring IR and VIS responses to different pulse durations of the stimuli and by measuring IR and VIS sensitivity thresholds on the variable photopic retinal illuminance backgrounds we demonstrated that a 2P process is responsible for IR vision. Robustness and the cost efficiency of the proposed system can be optimized in the future by using compact fiber-based short pulse lasers instead of expensive solid-state femtosecond lasers. It has been already demonstrated that fiber-based lasers produce sub-picosecond pulses in the desired range of optical frequencies [34]. It is also worth mentioning that further optimization of pulse length toward longer pulses will make the system less sensitive to dispersion introduced by ocular media.

Dark adaptation measurements revealed the differences between IR and VIS stimuli. Previously, delayed rod-mediated dark adaption has been associated with early AMD [2]. Moreover, individuals with delayed rod-mediated dark adaptation were found to be twice as likely to develop AMD, 3 years after their initial evaluation as compared to those subjects without delayed dark adaptation after the same period [2]. Delay of rod-mediated dark adaptation has also been associated with retinitis pigmentosa (RP) [35]. Finally, slower rates of dark adaptation with advancing age also have been reported for cones [36,37].

Considering the dark adaptation curves presented in Fig. 3(e) and Fig. 5, the relative difference between rods and cones was smaller for two-photon induced light perception than for normal vision. Consequently, the cone phase was relatively longer in the IR recovery plot in comparison to the VIS plot in the dark adaptation experiments. Although our experiments do not provide a conclusive explanation of this observation, this effect is likely related to the shifted spectral sensitivity of green/red cones (~530 and 560 nm, respectively) compared to rods (500 nm), making them more likely to undergo 2P activation by 1040 nm stimulation. Conveniently, the longer cone phase of dark adaptation should enable an expanded study of cone function with IR light. Observed differences between rod and cone plateaus in dark adaptation measurements are also evidence that perception of pulsed infrared stimuli is not simply caused by visible light produced in retinal tissue by other optical nonlinear process, e.g. second harmonic generation. The pulsed infrared stimuli, although seen as green, was due to infrared light activating the retina by two-photon absorption.

One possible explanation of this phenomenon is based on the finding that two-photon absorption probability depends strongly on light flux density. Photoreceptors are believed to act as waveguides, however, because of differences in size and shape, cones might be more effective than rods in collecting light, especially for a two photon process that requires well-defined localization of the delivered stimulus. It would result in higher flux density at cone outer segments than at rod outer segments. Another possible explanation is that the highest probability of absorption is different for cones and rods, meaning that the wavelength-dependent cross-section for the two photon absorption process can be different for cone opsins than for rhodopsin, considering the

Biomedical Optics EXPRESS

shifted spectral sensitivity of green/red cones (~530 and 560 nm, respectively) compared to rods (500 nm), Hence, the efficiency of the process may vary, and it can be reflected by the difference in the relaxation times.

Furthermore, we observed preservation of the visual stimulation pattern generated with IR but not with VIS light in lens opacities mimicking age-related effects (Fig. 4).

5. Conclusions

Our newly developed method enabled 2P excitation of visual pigments with IR light and measurements of visual sensitivity in humans within well-defined, focal regions of the retina.

Findings presented in this manuscript demonstrate that a newly developed method and instrumentation are capable of providing new results that are unique for two photon vision and that cannot be explained by a simple extrapolation based on the existing knowledge of normal visual processing. Yet, there is further need for additional tests – for example to explain the delay in the recovery time for the cone phase observed in our IR recovery plot and differences between rod and cones in visual sensitivity thresholds and in the dark adaptation measurements.

Based on the psychophysical data presented here, the technique could be used to obtain colocalized structural and functional measurements for patients suffering from eye diseases such as AMD, RP and cataract.

Funding

National Institutes of Health (EY019312, EY025451, EY027283); Research to Prevent Blindness; Gavin Herbert Eye Institute and the Department of Ophthalmology, University of California, Irvine; Department of Ophthalmology and Visual Sciences at Washington University; Narodowe Centrum Nauki (2016/23/B/ST2/00752); City of Gdynia (3/DOT/2016); Horizon 2020 Framework Programme (666295); Fundacja na rzecz Nauki Polskiej (TEAM TECH/2016-3/20).

Acknowledgements

M.W. acknowledges to: European Union, Polish Ministry of Science and Foundation for Polish Science. K.P. acknowledges to National Institutes of Health. K.P. is Chief Scientific Officer of Polgenix, Inc. K.K. acknowledges to the National Science Centre and to the City of Gdynia. V.J.K. acknowledges to the Department of Ophthalmology and Visual Sciences at Washington University and by Research to Prevent Blindness. We thank the members of the Palczewski laboratory for valuable comments regarding this manuscript. This work was partially carried out at the Department of Pharmacology, Case Western Reserve University, Cleveland, Ohio, USA. We also acknowledge Krzysztof Dalasinski for technical support, Karolina Kiluk for help with the dark adaptation measurements, and the contribution of human donor eye lenses from Dr. Irina Pikuleva.

Disclosures

GP: (P, E), MN: AM2M (E), PS: (P), KK (P), MW (P), KP: Polgenix, Inc. (C, S)

References

1. M. Crossland, M.-L. Jackson, and W. H. Seiple, "Microperimetry: a review of fundus related perimetry," Optometry Rep. **2**(1), 2 (2012).
2. C. Owsley, G. McGwin, M. E. Clark, G. R. Jackson, M. A. Callahan, L. B. Kline, C. D. Witherspoon, and C. A. Curcio, "Delayed Rod-Mediated Dark Adaptation Is a Functional Biomarker for Incident Early Age-Related Macular Degeneration," Ophthalmology **123**(2), 344–351 (2016).
3. G. Landa, E. Su, P. M. Garcia, W. H. Seiple, and R. B. Rosen, "Inner segment–outer segment junctional layer integrity and corresponding retinal sensitivity in dry and wet forms of age-related macular degeneration," Retina **31**(2), 364–370 (2011).

Biomedical Optics EXPRESS

4. J. H. Acton, N. S. Bartlett, and V. C. Greenstein, "Comparing the Nidek MP-1 and Humphrey field analyzer in normal subjects," Optom. Vis. Sci. **88**(11), 1288–1297 (2011).
5. F. K. Chen, P. J. Patel, W. Xing, C. Bunce, C. Egan, A. T. Tufail, P. J. Coffey, G. S. Rubin, and L. Da Cruz, "Test–Retest Variability of Microperimetry Using the Nidek MP1 in Patients with Macular Disease," Invest. Ophthalmol. Visual Sci. **50**(7), 3464–3472 (2009).
6. K. Rohrschneider, M. Becker, H. Krastel, F. Kruse, H. Völcker, and T. Fendrich, "Static fundus perimetry using the scanning laser ophthalmoscope with an automated threshold strategy," Graefe's Arch. Clin. Exp. Ophthalmol. **233**(12), 743–749 (1995).
7. S. N. Markowitz and S. V. Reyes, "Microperimetry and clinical practice: an evidence-based review," Can. J. Ophthalmol. **48**(5), 350–357 (2013).
8. W. S. Tuten, P. Tiruveedhula, and A. Roorda, "Adaptive optics scanning laser ophthalmoscope-based microperimetry," Optom. Vis. Sci. **89**(5), 563–574 (2012).
9. L. C. Sincich, Y. Zhang, P. Tiruveedhula, J. C. Horton, and A. Roorda, "Resolving single cone inputs to visual receptive fields," Nat. Neurosci. **12**(8), 967–969 (2009).
10. E. A. Rossi and A. Roorda, "The relationship between visual resolution and cone spacing in the human fovea," Nat. Neurosci. **13**(2), 156–157 (2010).
11. N. K. Cassels, J. M. Wild, T. H. Margrain, V. Chong, and J. H. Acton, "The use of microperimetry in assessing visual function in age-related macular degeneration," Surv. Ophthalmol. **63**(1), 40–55 (2018).
12. G. Palczewska, F. Vinberg, P. Stremplewski, M. P. Bircher, D. Salom, K. Komar, J. Zhang, M. Cascella, M. Wojtkowski, V. J. Kefalov, and K. Palczewski, "Human infrared vision is triggered by two-photon chromophore isomerization," Proc. Natl. Acad. Sci. U. S. A. **111**(50), E5445–E5454 (2014).
13. D. Mustafi, A. H. Engel, and K. Palczewski, "Structure of cone photoreceptors," Prog. Retinal Eye Res. **28**(4), 289–302 (2009).
14. C. A. Curcio, K. R. Sloan Jr., O. Packer, A. E. Hendrickson, and R. E. Kalina, "Distribution of cones in human and monkey retina: individual variability and radial asymmetry," Science **236**(4801), 579–582 (1987).
15. C. A. Curcio, K. R. Sloan, R. E. Kalina, and A. E. Hendrickson, "Human photoreceptor topography," J. Comp. Neurol. **292**(4), 497–523 (1990).
16. R. H. Masland, "The neuronal organization of the retina," Neuron **76**(2), 266–280 (2012).
17. J. Ambati and B. J. Fowler, "Mechanisms of age-related macular degeneration," Neuron **75**(1), 26–39 (2012).
18. C. Rivolta, D. Sharon, M. M. DeAngelis, and T. P. Dryja, "Retinitis pigmentosa and allied diseases: numerous diseases, genes, and inheritance patterns," Hum. Mol. Genet. **11**(10), 1219–1227 (2002).
19. F. LaRocca, A. H. Dhalla, M. P. Kelly, S. Farsiu, and J. A. Izatt, "Optimization of confocal scanning laser ophthalmoscope design," J. Biomed. Opt. **18**(7), 076015 (2013).
20. M. M. Thomas and T. D. Lamb, "Light adaptation and dark adaptation of human rod photoreceptors measured from the a-wave of the electroretinogram," J. Physiol. **518**(2), 479–496 (1999).
21. C. H. Graham, *Vision and visual perception* (Wiley, New York, 1965), pp. vii, 637 p.
22. B. Treutwein and H. Strasburger, "Fitting the psychometric function," Perception and Psychophysics **61**(1), 87–106 (1999).
23. B. Treutwein, "Adaptive psychophysical procedures," Vision Res. **35**(17), 2503–2522 (1995).
24. J. M. Bland and D. G. Altman, "Statistical methods for assessing agreement between two methods of clinical measurement," Lancet **327**(8476), 307–310 (1986).
25. A. Anastasakis, J. J. McAnany, G. A. Fishman, and W. H. Seiple, "Clinical value, normative retinal sensitivity values, and intrasession repeatability using a combined spectral domain optical coherence tomography/scanning laser ophthalmoscope microperimeter," Eye (London, U. K.) **25**(2), 245–251 (2011).
26. J. D. Hunter, "Matplotlib: A 2D graphics environment," Comput. Sci. Eng. **9**(3), 90–95 (2007).
27. A. World Medical, "World Medical Association Declaration of Helsinki: ethical principles for medical research involving human subjects," JAMA **310**(20), 2191–2194 (2013).
28. W. Denk, J. H. Strickler, and W. W. Webb, "Two-photon laser scanning fluorescence microscopy," Science **248**(4951), 73–76 (1990).
29. A. B. Watson, "QUEST plus : A general multidimensional Bayesian adaptive psychometric method," Journal of Vision **17**(3), 10 (2017).
30. T. D. Lamb and E. N. Pugh Jr., "Dark adaptation and the retinoid cycle of vision," Prog. Retinal Eye Res. **23**(3), 307–380 (2004).
31. E. A. Boettner and J. R. Wolter, "Transmission of the Ocular Media," Invest. Ophthalmol. Visual Sci. **1**, 776–783 (1962).
32. M. Hammer, A. Roggan, D. Schweitzer, and G. Muller, "Optical-Properties of Ocular Fundus Tissues - an in-Vitro Study Using the Double-Integrating-Sphere Technique and Inverse Monte-Carlo Simulation," Phys. Med. Biol. **40**(6), 963–978 (1995).
33. N. Domdei, L. Domdei, J. L. Reiniger, M. Linden, F. G. Holz, A. Roorda, and W. M. Harmening, "Ultra-high contrast retinal display system for single photoreceptor psychophysics," Biomed. Opt. Express **9**(1), 157–172 (2018).
34. J. Szczepanek, T. M. Kardas, M. Michalska, C. Radzewicz, and Y. Stepanenko, "Simple all-PM-fiber laser mode-locked with a nonlinear loop mirror," Opt. Lett. **40**(15), 3500–3503 (2015).

Biomedical Optics EXPRESS

35. R. Omar and P. Herse, "Quantification of dark adaptation dynamics in retinitis pigmentosa using non-linear regression analysis," Clinical & Experimental Optometry **87**(6), 386–389 (2004).
36. A. J. Gaffney, A. M. Binns, and T. H. Margrain, "Aging and cone dark adaptation," Optom. Vis. Sci. **89**(8), 1219–1224 (2012).
37. D. C. Coile and H. D. Baker, "Foveal dark adaptation, photopigment regeneration, and aging," Vis. Neurosci. **8**(1), 27–39 (1992).